ACS OMEGA

http://pubs.acs.org/journal/acsodf

Article

Implementing Contact Angle Hysteresis in Moving Mesh-Based Two-Phase Flow Numerical Simulations

Zheren Cai and Yanlin Song*

Cite This: *ACS Omega* 2021, 6, 35711−35717

Read Online

ACCESS | Metrics & More | Article Recommendations | Supporting Information

ABSTRACT: Contact angle hysteresis is a common phenomenon in nature, which also plays an important role in industrial applications. A numerical model based on the moving mesh two-phase flow method is presented for modeling contact angle hysteresis. The implementation includes a displacement-based penalty method and a state variable method. The pinning, moving, and repinning of the contact lines can be simulated. This method is robust considering both two-dimensional and three-dimensional geometries. To further demonstrate the performance of this method, a fluid−solid interaction model with a cylinder fluctuating on a water surface considering contact angle hysteresis is demonstrated.

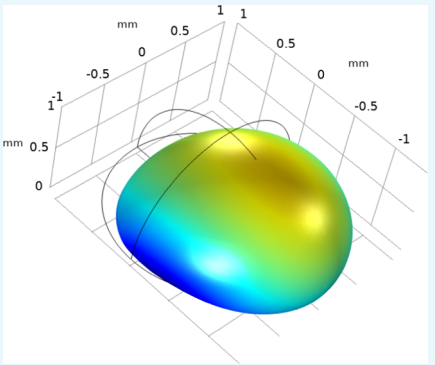

INTRODUCTION

The contact angle (CA) for a liquid droplet on a solid surface is commonly used to characterize the wettability of the solid surface.[1] The classical Young's equation provides a unique CA when the three-phase system is in a static state with the lowest global surface energy. However, solid surfaces can hardly be perfectly homogeneous and smooth because most of them are covered with natural defects, rough structures, or artificial patterns, where the apparent contact angle is generally different from the equilibrium CA.[2−4] The CA when the interface is moving forward (called the advancing CA) is larger than that when moving backward (called the receding CA). The difference between the advancing CA and the receding CA is defined as contact angle hysteresis (CAH).[1,4−6] CAH is one of the most common phenomena in nature, which also plays an important role in industrial applications such as immersion lithography, fiber coatings, and inkjet printing.[2] Recently, many digital microfluidics[7−9] take advantage of surface wetting phenomena to achieve droplet manipulations and drug delivery. Numerical simulation is a powerful tool to help design these microfluidic devices. However, because of the complexity of CAH modeling, the CAH is usually ignored in these simulations for microfluidic designs.[10] Thus, developing numerical methods to model the CAH phenomenon is an important topic in computational fluid dynamics (CFD).

The simulations of droplet motion require a two-phase flow model, where the shape of the droplet interface is explicitly presented. The finite volume method or finite element method CFD solvers for these kinds of two-phase flow can be classified into two types. The first type is field-based methods including the volume of fluid (VOF) method,[11] level-set method,[12,13] or phase-field method,[14] which distinguishes the two-phase flow using an additional field variable. The second type is the moving mesh method,[15] which uses the deforming mesh to describe the shape of the interface. In some works,[16−19] the authors implement CAH using the first type of two-phase flow model. Fang et al. carried out a transient model by correcting boundary force balances through specifying the local CA and instantaneously updating the local angle values based on the variation of the volume fraction from previous time steps.[16] Dupont et al. carried out the numerical method based on the implementation of a "subgrid" description of the contact line that consists in imposing the apparent angle for static and moving contact lines.[17] The model reported by Ahmed et al. automatically locates the advancing and receding sections of the contact line, which enables the application of different contact angles at the advancing and receding fronts and therefore takes into account CAH.[18] In the model of He et al., a pair of pseudoline tensions in the receding and advancing states, respectively, are utilized to represent contact line interactions with the substrate.[19]

Here, we provide a method to implement CAH in a moving mesh-based two-phase flow CFD solver. With the moving mesh approach, the phase boundary is modeled as a geometrical surface separating two domains, with one phase

Received: October 8, 2021
Accepted: December 8, 2021
Published: December 17, 2021

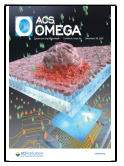

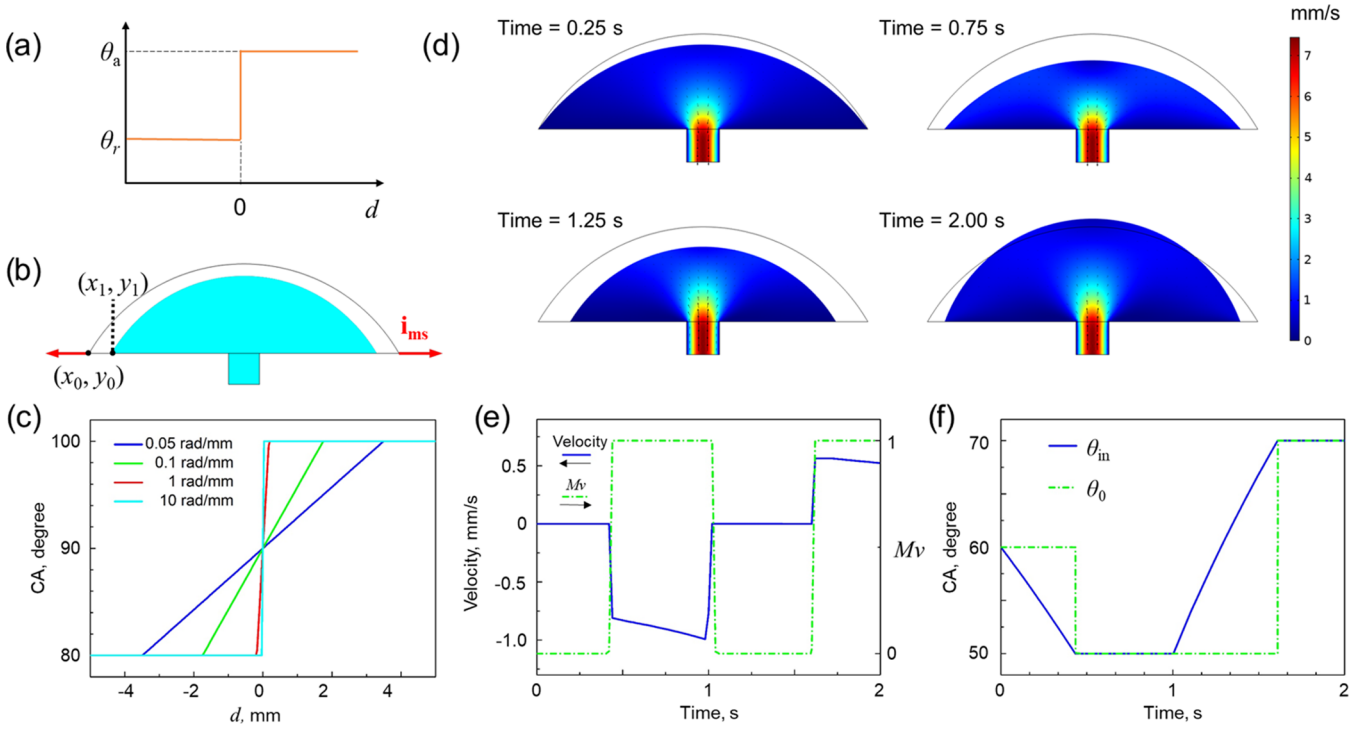

Figure 1. Numerical method demonstration in 2D. (a) CA versus contact line displacement of CAH. (b) Modeling scheme with the black curve indicating the initial shape of the droplet and $\mathbf{i}_{ms}$ is the unit surface binormal vector. (c) Plots of eq 3 with different p values. (d) Velocity distributions and shape deformations of the droplet. (e) Simulation results of contact point moving velocity and Mv corresponding to panel (d). (f) Simulation results of θ_0 and θ_{in} corresponding to panel (d).

at each side in the corresponding domains. The shape of the interface is more accurate compared to field-based methods. Forces and fluxes can be directly applied on the phase boundary. An advantage of the moving mesh method is that it can model one single phase while the other phase can be ignored. The drawback of the moving mesh model is that it cannot deal with topology changes.[15,20] This work is based on a commercial CFD solver provided by COMSOL Multiphysics (abbreviated as COMSOL). The "two-phase flow moving mesh" interface in COMSOL only provides the condition of a simple CA that follows the Young's equation.[21,22] This work provides a method to implement CAH in COMSOL. The core idea of this method is based on the penalty method.[23,24] The advancing and receding CA are the input parameters in the simulations. The pinning, moving, and repinning of the contact line can be simulated. This method is robust in simulations considering both two-dimensional (2D) and three-dimensional (3D) geometries. To further demonstrate the performance of this method, we conduct a fluid−solid interaction (FSI) simulation, where a cylinder is fluctuating on a water surface, where the contact line exhibits CAH.

RESULTS AND DISCUSSION

Numerical Models and Methods. The main characteristic of CAH is that the contact line is pinning at the initial position when the apparent CA is less than the advancing CA and larger than the receding CA. The contact lines begin to move as the apparent CA reaches advancing CA (θ_a) or receding CA (θ_r). The relation between the apparent CA and the displacement of the contact line is plotted in Figure 1a. We use a penalty method to describe the pinning characteristics. First, we use a 2D geometry to demonstrate this method. As shown in Figure 1b, a droplet is placed on a surface with a channel at the bottom to inject or remove liquid to or from the droplet. We define the input CA (θ_{in}) as a function of the displacement (d) of the contact point, i.e.,

$$\theta_{in} = \theta_0 + pd \tag{1}$$

where θ_0 is the initial CA and p is the penalty parameter being positive. The displacement (d) is defined as

$$d = (x_1 - x_0, y_1 - y_0)\cdot\mathbf{i}_{ms} \tag{2}$$

where $\mathbf{i}_{ms}$ is the unit surface binormal vector as shown in Figure 1b, (x_0, y_0) is the initial position of the contact point, and (x_1, y_1) is the current position of the contact point after moving. When the contact point is advancing, the value of d is positive and θ_{in} will become larger to prevent the contact point from advancing any further. When the contact point is receding, the value of d is negative and θ_{in} will become smaller to prevent the contact point from receding any further. When p is big enough, the value of d is very close to zero as the value of CA changes from θ_a to θ_r. Thus, eq 1 makes the contact point pinning at the initial position (x_0, y_0). Based on eq 1, we construct an inequality relation to constrain the maximum and minimum values of θ_{in}.

$$\theta_{in} = \begin{cases} \theta_a, & \theta_0 + pd \geq \theta_a \\ \theta_0 + pd, & \theta_r < \theta_0 + pd < \theta_a \\ \theta_r, & \theta_0 + pd \leq \theta_r \end{cases} \tag{3}$$

Then, θ_{in} will not become larger than θ_a or smaller than θ_r. The contact point will start to move as θ_{in} reaches θ_a or θ_r. We plot eq 3 in Figure 1c with different values of p while the values of θ_0, θ_a, and θ_r are 90, 100, and 80°, respectively. When p is big

https://doi.org/10.1021/acsomega.1c05613
ACS Omega 2021, 6, 35711−35717

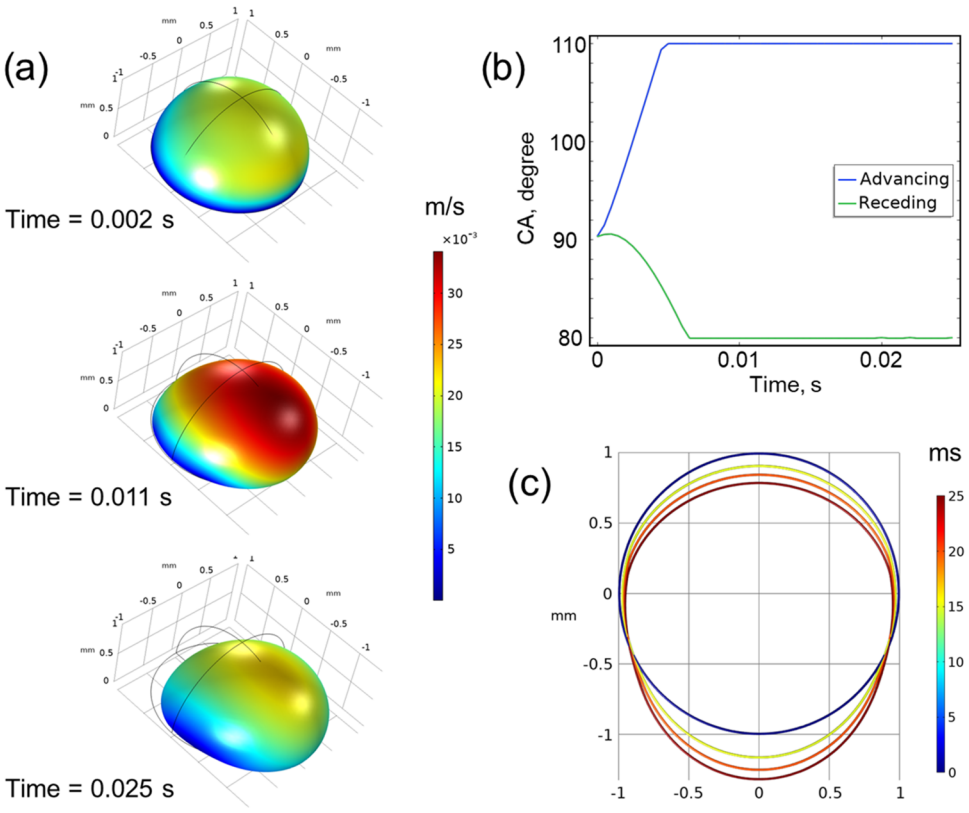

Figure 2. Modeling of a sliding droplet: (a) Simulation results with the color presenting the velocity, (b) advancing CA and receding CA over time, and (c) contact line profiles over time.

enough, the curve is nearly the same as in Figure 1a. Thus, eq 3 can be used to simulate CAH.

Some refs 2, 17, 25 reported that the apparent CA varies with the moving velocity of the contact point (v_c). To include this effect, an additional velocity-dependent function, $f(v_c)$, can be added to describe this dynamic CA.

$$\theta_{in} = \begin{cases} \theta_a + f(v_c), & \theta_0 + pd \geq \theta_a \\ \theta_0 + pd, & \theta_r < \theta_{in} + pd < \theta_a \\ \theta_r + f(v_c), & \theta_0 + pd \leq \theta_r \end{cases} \quad (4)$$

The wetting behavior varies for different liquids and different substrates. It depends on the experimental observations whether the velocity-dependent CA requires to be considered in the simulations. In this work, we only use eq 3, where the velocity-dependent CA change is ignored.

When the CA reaches θ_a or θ_r, the contact point starts to move. Then, when the contact point stops, it will be pinned again in a new position. To describe the repinning process, the coordinates of the position (x_0, y_0) need to be updated. To simplify the formulas, we define a bool variable, Mv.

$$Mv = \begin{cases} 0, & \theta_r < \theta_0 + pd < \theta_a \\ 1, & \theta_0 + pd \geq \theta_a \text{ or } \theta_0 + pd \leq \theta_r \end{cases} \quad (5)$$

Mv equals 1 when the contact point is moving and 0 otherwise. Then, the position (x_0, y_0) is defined as a state variable

$$(x_0, y_0) = \begin{cases} (x_0, y_0), & Mv = 0 \\ (x_1, y_1), & Mv = 1 \end{cases} \quad (6)$$

When the contact point is pinning, the value of (x_0, y_0) keeps unchanged. When the contact point is moving, the pinning position is updated to be the current position. To avoid the eruptive change of θ_{in}, θ_0 also needs to be defined as a state variable and is updated when Mv is 1.

$$\theta_0 = \begin{cases} \theta_0, & Mv = 0 \\ \theta_{in}, & Mv = 1 \end{cases} \quad (7)$$

Using the above settings, we simulate such a process that the water is first drained out of the droplet and then injected into the droplet. The governing equations for the incompressible fluid flow are

$$\rho\frac{\partial \mathbf{u}}{\partial t} + \rho(\mathbf{u}\cdot\nabla)\mathbf{u} = \nabla\cdot[-p_s\mathbf{I} + \mu(\nabla\mathbf{u} + (\nabla\mathbf{u})^T)] \quad (8)$$

$$\rho\nabla\cdot\mathbf{u} = 0 \quad (9)$$

where $\mathbf{u}$ is the velocity, ρ is the density, p_s is the pressure, μ is the dynamic viscosity, and t is the time. The equation for the droplet surface is

$$\mathbf{n}\cdot[-p_s\mathbf{I} + \mu(\nabla\mathbf{u} + (\nabla\mathbf{u})^T)] = \sigma(\nabla_t\cdot\mathbf{n})\mathbf{n} - \nabla_t\sigma \quad (10)$$

where σ is the surface tension and $\mathbf{n}$ is the surface normal vector. The moving mesh provided by COMSOL will automatically deform the mesh to adapt the shape of the droplet. The numerical solver in COMSOL will apply a force at the contact point to maintain the apparent CA of the droplet

https://doi.org/10.1021/acsomega.1c05613
ACS Omega 2021, 6, 35711−35717

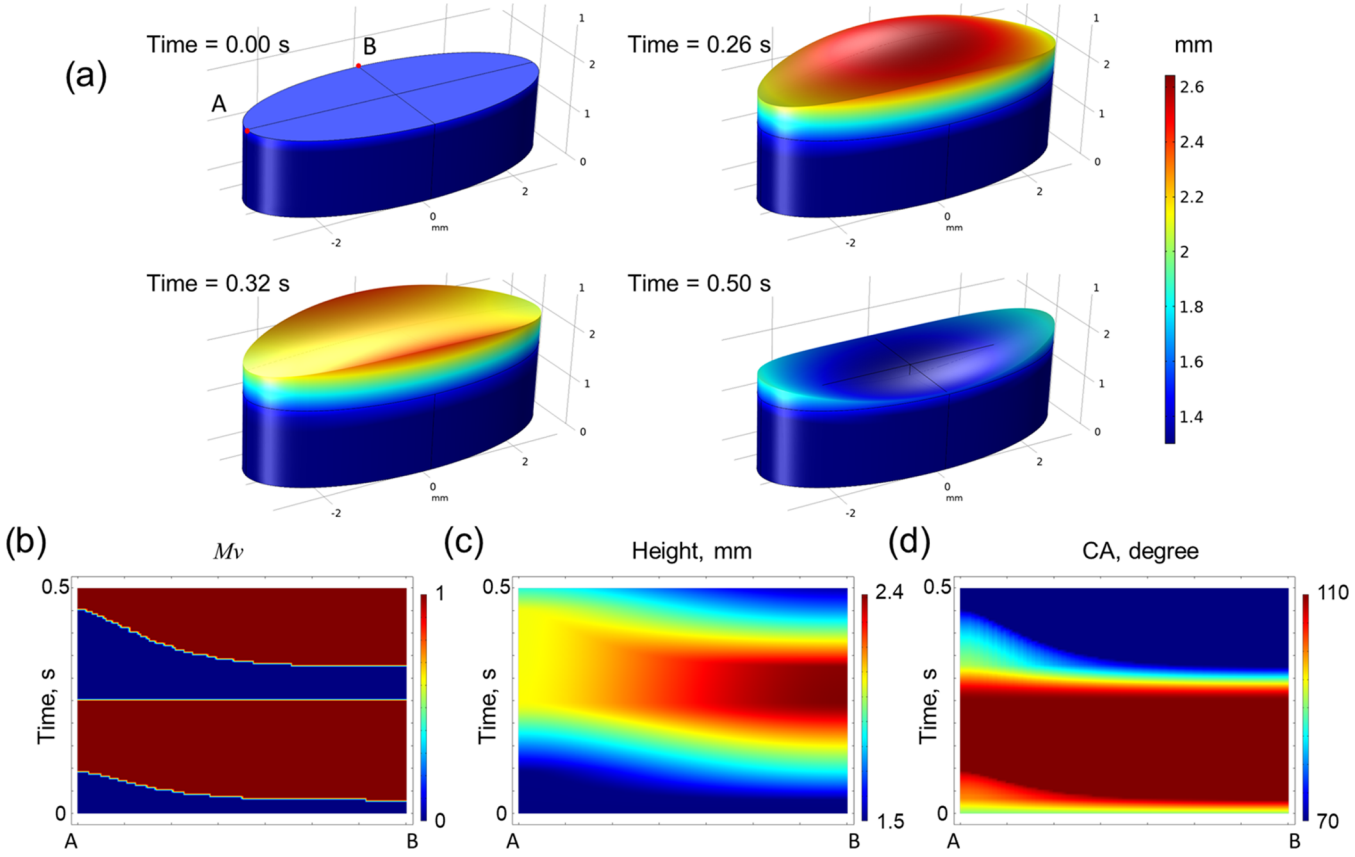

Figure 3. Modeling of a liquid surface rising and falling in an ellipse tube: (a) Simulation results with the color presenting the height of the surface, (b) *Mv* distributions along arc AB, (c) surface height distributions along arc AB, and (d) apparent CA distributions along arc AB.

to be the input CA. As for the example in Figure 1d, the initial CA is 60°. The advancing and receding CA is 70 and 50°, respectively. The initial distance between the two contact points is 5 mm. The material of the droplet is water, with its parameters taken from the built-in library in COMSOL. The instructions for implementing eqs 1−7 in COMSOL are provided in Figures S1−S3. The simulation results are shown in Figure 1d and Movie S1. Figure 1e shows the time-dependent plots of contact point moving velocity and the bool variable, *Mv*. Figure 1f shows the time-dependent plots of θ_0 and θ_{in}. The contact point goes through four processes, namely, pinning, moving, repinning, and moving. In the first process, *Mv* is 0 and θ_0 keeps unchanged while θ_{in} decreases. In the second process, *Mv* turns into 1 and θ_0 turns into θ_r since the contact point moves. In this process, the state variables θ_0 and (x_0, y_0) are updated in every numerical time step. As θ_{in} cannot be smaller than θ_r, the value of θ_0 is always θ_r. The value of (x_0, y_0) is the output value of (x_1, y_1) in the last time step of the current process and is the input parameter for the simulation in the next time step. If the output value of (x_1, y_1) makes a negative value of d in the next time step, $\theta_0 + pd$ will be less than θ_r. Then, *Mv* is still 1. If the output value of (x_1, y_1) makes a positive value of d in the next time step, $\theta_0 + pd$ will be larger than θ_r, which means that the moving direction of the contact point is changed. Then, *Mv* is 0, and the state variable stops updating. Thus, the contact point is pinning again, which is described as the third process. In the fourth process, $\theta_0 + pd$ is larger than θ_a, and the contact point is moving again. Thus, the CAH is successfully simulated.

3D CAH Simulations. Here, we demonstrate two 3D CAH examples. In 3D, the contact points become contact lines. Every contact point at the contact line has a value of CA. The implementing methods in 3D and 2D are similar. The only difference is that the coordinates of contact points and the vectors have three components in 3D.

The first example is a hemispheric droplet sliding down a ramp. The ramp has a gradient of 45°. The acceleration of gravity is 9.8 m/s^2. The radius of the droplet is 1 mm. The initial CA is 90°. The density and viscosity of the liquid are 998.2 kg/m^3 and 0.02 Pa·s, respectively. The surface tension is 0.01 N/m. The advancing and receding CAs are 110 and 80°, respectively. The initial shape of the droplet is hemispherical, and its deformation and movement are shown in Figure 2a and Movie S2. Figure 2b shows the time-dependent plots of the advancing CA and receding CA. The instructions for implementing CAH of this example in COMSOL are provided in Figures S4−S6. Figure 2c shows the profile change of the contact line over time. The results are qualitatively agreeable with experimental observations in the refs 18, 19.

The second example is the rising and falling of a liquid surface in a tube with an elliptical cross section. The long axis and short axis of the ellipse are 6 and 2.6 mm, respectively. The initial CA is 90°. The advancing and receding CAs are 110 and 70°, respectively. The density and viscosity of the liquid are 998.2 kg/m^3 and 0.01 Pa·s, respectively. The surface tension is 0.07 N/m. The inlet and outlet velocity are both 4 mm/s. The instructions for implementing CAH of this example in COMSOL are provided in Figures S7−S9. The results are presented in Figure 3a and Movie S3. As shown in Figure 3a,

https://doi.org/10.1021/acsomega.1c05613
ACS Omega 2021, 6, 35711−35717

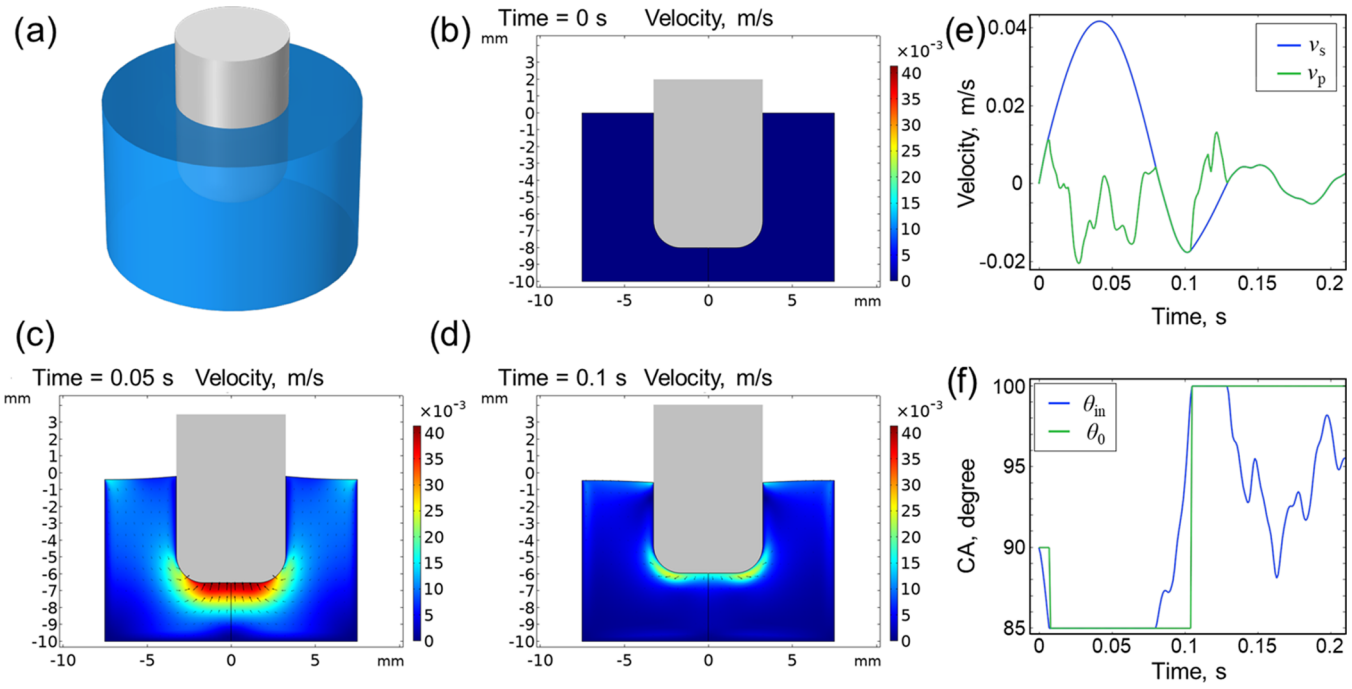

Figure 4. FSI simulation: (a) Cylinder floating on the water surface, (b–d) simulation results with the color presenting the velocity, (e) simulation results of the velocities of the cylinder (v_s) and the contact point (v_p), and (f) simulation results of θ_0 and θ_{in}.

we define two points, namely, A and B at the contact line. The time-dependent distributions of variable Mv, height of the contact line, and CA along the contact line from A to B are plotted in Figure 3b–d, respectively. The abscissa is the arc length and the ordinate is time, and the variable values are presented by colors. Because of the elliptical shape, it is easier to reach point B, advancing CA and receding CA. Thus, point B starts moving first and then point A finally starts to move. These two examples show that this method can be well applied to 3D cases.

Fluid–Solid Interaction Simulation with CAH. To further demonstrate the performance of this method, we conduct an FSI simulation with CAH. Compared with a previous simulation, the difference here in the FSI simulation is that the solid surface also moves. The relative displacements need to be calculated. Here, we simulate a cylinder floating on the water surface (Figure 4a). The density of the cylinder is 600 kg/m^3. The cylinder is pressed into the water at the beginning. After releasing, the cylinder is floating up and down. The initial CA is 90°, with the advancing and receding CAs of 100 and 85°, respectively. In the simulation, 2D axisymmetric space dimension is used. The cylinder is considered as a rigid body. The cylinder is subjected to the gravitational force, fluid force, and surface tension force. The acceleration of the cylinder (a_s) can be written as

$$a_s = -g - \frac{\int \sigma \cos(\theta_{in})\mathrm{d}x}{m_s} + \frac{\iint T\mathrm{d}s}{m_s} \tag{11}$$

where g is the acceleration of gravity, T is the fluid force acting on the solid surface per area calculated by COMSOL, θ_{in} is the apparent CA, m_s is the mass of the cylinder, and σ is the surface tension. The instructions for implementing eq 11 in COMSOL are provided in Figure S10. The velocity of the cylinder (v_s) is

$$v_s = \int a_s \mathrm{d}t \tag{12}$$

The displacement of the cylinder (D_s) is

$$D_s = \int v_s \mathrm{d}t \tag{13}$$

The instructions for implementing eqs 12 and 13 in COMSOL are provided in Figure S11. Then, D_s is used to control the deformation of the fluid domain. The instructions for implementing the deformation of the fluid domain in COMSOL are provided in Figure S12. In this model, the cylinder can only move in a vertical direction (z direction). We take an arbitrary point in the cylinder to trace its movement. The initial z coordinate of this point is z_{s0}, and the current z coordinate is z_{s1}. The displacement of the cylinder (d_s) can be defined as

$$d_s = z_{s1} - z_{s0} \tag{14}$$

Then, the displacement of the contact point on the cylinder surface (d_c) is

$$d_c = z_{c1} - z_{c0} - d_s \tag{15}$$

where z_{c0} is the initial z coordinate of the contact point and z_{c1} is the current z coordinate of the contact point. Then, the input CA can be defined.

$$\theta_{in} = \begin{cases} \theta_a, & \theta_0 + pd_c \geq \theta_a \\ \theta_0 + pd_c, & \theta_r < \theta_0 + pd_c < \theta_a \\ \theta_r, & \theta_0 + pd_c \leq \theta_r \end{cases} \tag{16}$$

To simulate the repinning of the contact point, z_{c0}, θ_0, and z_{s0} need to be defined as state variables.

$$z_{c0} = \begin{cases} z_{c0}, & Mv = 0 \\ z_{c1}, & Mv = 1 \end{cases} \tag{17}$$

https://doi.org/10.1021/acsomega.1c05613
ACS Omega 2021, 6, 35711–35717

$$z_{s0} = \begin{cases} z_{s0}, & Mv = 0 \\ z_{s1}, & Mv = 1 \end{cases} \quad (18)$$

$$\theta_0 = \begin{cases} \theta_0, & Mv = 0 \\ \theta_{in}, & Mv = 1 \end{cases} \quad (19)$$

In FSI simulations, the displacements of the solid surface also need to be updated when depinning occurs. The instructions for implementing eqs 14−19 in COMSOL are provided in Figures S13−S15.

Using the above settings, the FSI with CAH is simulated. The results are shown in Figure 4b−d and Movie S4. Figure 4e shows the moving velocity of a cylinder (v_s) and the contact point (v_p). When the two curves are overlapping, the relative velocity between the cylinder and contact point is zero, indicating the pinning of the contact point at the cylinder surface. The time-dependent values of θ_0 and θ_{in} are shown in Figure 4f. When the contact point is pinning, the values of θ_0 and θ_{in} are different. From these results, we can see that FSI with CAH is successfully simulated.

CONCLUSIONS

In this paper, a method of implementing CAH in a moving mesh-based two-phase flow model has been presented and verified with several examples. This method is based on the displacement of the contact lines. It takes advantage of easily obtaining the coordinates of the contact lines in the moving mesh method. The penalty method is used to pin the contact line at a given position. The maximum and minimum values of the input CA are constrained to be the advancing and receding CAs. The repinning of the contact line is realized using the state variables to update the pinning positions. This method is robust when dealing with both 2D and 3D geometries and can be implemented in FSI simulations.

Some previous works[26,27] reported the velocity-based methods to describe the dynamic CA, where the CA is a function of the moving velocity of the contact line, which increases with the advancing velocity and decreases with the receding velocity. CAH can be mimicked by these methods. However, this method is difficult to model static CAH when the velocity of the contact line is zero. The velocity-dependent CA only gives one specific value when the velocity of the contact line is zero, which cannot describe the CA change when the contact line is pinning. Our displacement-based method can model static CAH when the contact line is pinning, and the velocity-based dynamic CA can also be incorporated in our method as shown in eq 4 when the contact line is moving. From a numerical calculation point of view, penalty methods based on the contact line displacement are usually easier to solve and have better convergence than those based on the contact line velocity, as velocity is the derivative of displacement with respect to time. Moreover, although this method is implemented in COMSOL in this work, it is possible to be applied in other CFD solvers.

In addition, the reported methods[3,16−19] for CAH are unfriendly for researchers who are not familiar with the sophisticated CFD solver and programming, which cannot benefit many researchers from applying them in microfluidics. This work provides a method to simulate CAH through the commercial software COMSOL without any coding. With the detailed modeling setups provided in the Supporting Information, this method can be replicated by other researchers easily.

ASSOCIATED CONTENT

Supporting Information

The Supporting Information is available free of charge at https://pubs.acs.org/doi/10.1021/acsomega.1c05613.

Nomenclatures; the instructions of implementing CAH in COMSOL; variable definitions in COMSOL; definitions of state variables in COMSOL; variable θ_{in} (theta_in) used in the boundary condition; definitions of the acceleration of the cylinder. Settings in the moving mesh (PDF)

Movie S1: Simulated results of contact angle advancing and receding (MP4)

Movie S2: Simulated results of 3D droplet sliding (MP4)

Movie S3: Simulation results of a liquid surface rising and falling in an elliptical tube (MP4)

Movie S4: Simulation results of fluid-solid interaction with contact angle hysteresis (MP4)

AUTHOR INFORMATION

Corresponding Author

Yanlin Song − *Key Laboratory of Green Printing, Institute of Chemistry, Chinese Academy of Sciences, 100190 Beijing, P. R. China; University of Chinese Academy of Sciences, 100049 Beijing, P. R. China;* orcid.org/0000-0002-0267-3917; Email: ylsong@iccas.ac.cn

Author

Zheren Cai − *Key Laboratory of Green Printing, Institute of Chemistry, Chinese Academy of Sciences, 100190 Beijing, P. R. China; University of Chinese Academy of Sciences, 100049 Beijing, P. R. China*

Complete contact information is available at: https://pubs.acs.org/10.1021/acsomega.1c05613

Author Contributions

Z.C. conducted all the work. Y.S. conceived and supervised the project.

Notes

The authors declare no competing financial interest.

ACKNOWLEDGMENTS

The authors thank Dr. Qin Feifei (Chair of Building Physics, Department of Mechanical and Process Engineering, ETH Zürich) for editing the language of the article. The authors thank the financial support of the National Key R&D Program of China (2018YFA0208501), the National Natural Science Foundation of China (NSFC, Nos. 51803217, 51773206, 91963212 and 51961145102), and K. C. Wong Education Foundation.

ABBREVIATIONS

CA, contact angle; CAH, contact angle hysteresis; CFD, computational fluid dynamics; VOF, volume of fluid; 2D, two-dimensional; 3D, three-dimensional; FSI, fluid−solid interaction

REFERENCES

(1) Koishi, T.; Yasuoka, K.; Fujikawa, S.; Zeng, X. C. Measurement of Contact-Angle Hysteresis for Droplets on Nanopillared Surface and in the Cassie and Wenzel States: A Molecular Dynamics Simulation Study. *ACS Nano* **2011**, *5*, 6834−6842.

(2) Eral, H. B.; T Mannetje, D. J. C. M.; Oh, J. M. Contact Angle Hysteresis: A Review of Fundamentals and Applications. *Colloid Polym. Sci.* **2013**, *291*, 247−260.

(3) Huang, J. J.; Huang, H.; Wang, X. Numerical Study of Drop Motion on a Surface with Stepwise Wettability Gradient and Contact Angle Hysteresis. *Phys. Fluids* **2014**, *26*, No. 062101.

(4) Wang, Y.; Zhao, J.; Zhang, D.; Jian, M.; Liu, H.; Zhang, X. Droplet Sliding: The Numerical Observation of Multiple Contact Angle Hysteresis. *Langmuir* **2019**, *35*, 9970−9978.

(5) Hong, S.-J.; Chang, F.-M.; Chou, T.-H.; Chan, S. H.; Sheng, Y.-J.; Tsao, H.-K. Anomalous Contact Angle Hysteresis of a Captive Bubble: Advancing Contact Line Pinning. *Langmuir* **2011**, *27*, 6890−6896.

(6) Qin, F.; Zhao, J.; Kang, Q.; Derome, D.; Carmeliet, J. Lattice Boltzmann Modeling of Drying of Porous Media Considering Contact Angle Hysteresis. *Transp. Porous Media* **2021**, *140*, 395−420.

(7) Wang, Q.; Xu, M.; Wang, C.; Gu, J.; Hu, N.; Lyu, J.; Yao, W. Actuation of a Nonconductive Droplet in an Aqueous Fluid by Reversed Electrowetting Effect. *Langmuir* **2020**, *36*, 8152−8164.

(8) Cooney, C. G.; Chen, C.-Y.; Emerling, M. R.; Nadim, A.; Sterling, J. D. Electrowetting Droplet Microfluidics on a Single Planar Surface. *Microfluid. Nanofluid.* **2006**, *2*, 435−446.

(9) Pollack, M. G.; Fair, R. B.; Shenderov, A. D. Electrowetting-Based Actuation of Liquid Droplets for Microfluidic Applications. *Appl. Phys. Lett.* **2000**, *77*, 1725.

(10) Wei, Q.; Yao, W.; Gu, L.; Fan, B.; Gao, Y.; Yang, L.; Zhao, Y.; Che, C. Modeling, Simulation, and Optimization of Electrowetting-on-Dielectric (EWOD) Devices. *Biomicrofluidics* **2021**, *15*, No. 014107.

(11) Ménard, T.; Tanguy, S.; Berlemont, A. Coupling Level Set/VOF/Ghost Fluid Methods: Validation and Application to 3D Simulation of the Primary Break-up of a Liquid Jet. *Int. J. Multiphase Flow* **2007**, *33*, 510−524.

(12) Olsson, E.; Kreiss, G.; Zahedi, S. A Conservative Level Set Method for Two Phase Flow II. *J. Comput. Phys.* **2007**, *225*, 785−807.

(13) Olsson, E.; Kreiss, G. A Conservative Level Set Method for Two Phase Flow. *J. Comput. Phys.* **2005**, *210*, 225−246.

(14) Yue, P.; Feng, J. J.; Liu, C.; Shen, J. A Diffuse-Interface Method for Simulating Two-Phase Flows of Complex Fluids. *J. Fluid Mech.* **2004**, *515*, 293−317.

(15) Scardovelli, R.; Zaleski, S. Direct Numerical Simulation of Free-Surface and Interfacial Flow. *Annu. Rev. Fluid Mech.* **1999**, *31*, 567−603.

(16) Fang, C.; Hidrovo, C.; Wang, F. min.; Eaton, J.; Goodson, K. 3-D Numerical Simulation of Contact Angle Hysteresis for Microscale Two Phase Flow. *Int. J. Multiphase Flow* **2008**, *34*, 690−705.

(17) Dupont, J. B.; Legendre, D. Numerical Simulation of Static and Sliding Drop with Contact Angle Hysteresis. *J. Comput. Phys.* **2010**, *229*, 2453−2478.

(18) Ahmed, G.; Sellier, M.; Jermy, M.; Taylor, M. Modeling the Effects of Contact Angle Hysteresis on the Sliding of Droplets down Inclined Surfaces. *Eur. J. Mech. B* **2014**, *48*, 218−230.

(19) He, P.; Yao, C. W. Simulating Contact Angle Hysteresis Using Pseudo-Line Tensions. *MRS Commun.* **2019**, *9*, 1060−1066.

(20) Gerbeau, J. F.; Lelièvre, T. Generalized Navier Boundary Condition and Geometric Conservation Law for Surface Tension. *Comput. Methods Appl. Mech. Eng.* **2009**, *198*, 644−656.

(21) Ren, W.; E, W. Boundary Conditions for the Moving Contact Line Problem. *Phys. Fluids* **2007**, *19*, No. 022101.

(22) Ren, W.; Hu, D.; E, W. Continuum Models for the Contact Line Problem. *Phys. Fluids* **2010**, *22*, No. 102103.

(23) Huněk, I. On a Penalty Formulation for Contact-Impact Problems. *Comput. Struct.* **1993**, *48*, 193−203.

(24) Weyler, R.; Oliver, J.; Sain, T.; Cante, J. C. On the Contact Domain Method: A Comparison of Penalty and Lagrange Multiplier Implementations. *Comput. Methods Appl. Mech. Eng.* **2012**, *205*−*208*, 68−82.

(25) Dussan, E. B. On the Spreading of Liquids on Solid Surfaces: Static and Dynamic Contact Lines. *Annu. Rev. Fluid Mech.* **1979**, *11*, 371−400.

(26) Šikalo, Š.; Wilhelm, H.-D.; Roisman, I. V.; Jakirlić, S.; Tropea, C. Dynamic Contact Angle of Spreading Droplets: Experiments and Simulations. *Phys. Fluids* **2005**, *17*, No. 062103.

(27) Roisman, Iv.; Opfer, L.; Tropea, C.; Raessi, M.; Mostaghimi, J.; Chandra, S. Drop Impact onto a Dry Surface: Role of the Dynamic Contact Angle. *Colloids Surf., A* **2008**, *322*, 183−191.

https://doi.org/10.1021/acsomega.1c05613
ACS Omega 2021, 6, 35711−35717